

# MUONS VERSUS HADRONS FOR RADIOTHERAPY \*

N. V. Mokhov<sup>†</sup>, and A. Van Ginneken, FNAL, Batavia, IL

## Abstract

Intense low energy muon beams – as part of a muon collider complex – may become available for use in radiotherapy. It is of interest to compare their effectiveness in this application with that of hadron beams in a setting where processes common to these beams are treated exactly alike. Detailed simulations of physics processes for muon, proton, antiproton, neutron, kaon and pion beams stopping in various media have been performed using the MARS code with newly developed weighted algorithms. Special attention is paid to  $\mu^-$ ,  $\pi^-$ , and  $\bar{p}$  capture on light nuclei. Calculated distributions of energy deposition and dose equivalent due to processes involving primary beams and generated secondaries are presented for a human tissue-equivalent phantom (TEP). The important ratio of dose delivered to healthy tissue *vs* dose to tumor is examined within this model. The possibility of introducing heavier elements into the tumor to increase capture of stopped  $\mu^-$  is briefly explored.

## 1 INTRODUCTION

Facilities needed for a muon collider[1] would provide an unprecedented variety of intense hadron and muon beams in an energy range well suited for radiotherapy. Hadron beams have been shown to offer certain advantages in cancer treatment compared to conventional photon radiotherapy[2]. To explore the potential of beams available at a muon collider, we have developed the coding necessary to simulate the detailed dose distributions associated with these beams. A large part of this effort concerns the processes occurring when particles are stopped. First results show that such beams can be used successfully in radiotherapy. Comparison of the effectiveness of various beams with each other and with simulations may offer valuable insight into this type of cancer treatment.

## 2 STOPPED HADRONS AND MUONS

A careful treatment of processes near and below the Coulomb barrier in hadron and muon transport has been implemented in MARS (stopping by ionization losses *vs* nuclear interaction *vs* decay).

### 2.1 Pions

A stopping  $\pi^+$  decays into  $\mu^+$  of 4.1 MeV plus a neutrino while a  $\pi^-$  attaches to a nucleus (via a modified Fermi-

Teller law). While cascading down the atomic energy levels the pion is captured predominantly from a high orbit thus only a few low energy photons are emitted (which may be neglected here). The hadronic interaction of the stopped  $\pi^-$  is treated using the Cascade-Exciton Model [4] with a few modifications. When hydrogen is the target it is assumed there is a 60% probability for charge exchange ( $\pi^-p \rightarrow \pi^0n$ ) whereupon the  $\pi^0$  decays into two photons of 68.9 MeV each and the neutron acquires a small (0.4 MeV) kinetic energy. The remaining 40% of stopped  $\pi^-$  in hydrogen interact via radiative capture:  $\pi^-p \rightarrow n\gamma$ . Here the photon acquires 129.4 MeV and the neutron 8.9 MeV kinetic energy. Other nuclides have a much smaller probability for radiative capture (1–2%) which is taken into account in competition with the non-radiative type as simulated by the CEM95 code. The photon energy is chosen from an empirical fit to experiment while the remainder is deposited as excitation energy.

### 2.2 Muons

A stopping  $\mu^+$  always decays into  $e\nu\bar{\nu}$  while a  $\mu^-$  attaches itself to a nucleus. When a  $\mu^-$  stops in a compound or mixture one first decides to which nucleus the  $\mu^-$  attaches (modified Fermi-Teller law). Following attachment the muon may still decay as decided by comparing capture and decay lifetimes of which the latter is favored for light nuclei ( $Z \leq 11$ ). A captured  $\mu^-$  then cascades down to the ground state of the muonic atom emitting photons along with some Auger electrons, all of which is simulated using approximate fits to the atomic energy levels. In hydrogen  $\mu^-$  capture always produces a 5.1 MeV neutron via inverse  $\beta$ -decay. In complex nuclei the giant dipole resonance plays a role and results in an ‘evaporation’-type neutron spectrum with one or more resonances superimposed. In addition smaller numbers of evaporation-type charged particles and photons may be emitted.

### 2.3 Antiprotons

Stopped  $\bar{p}$  attach to nuclei in the same way as  $\pi^-$  or  $\mu^-$ . Annihilation at rest is assumed to produce only pions, neglecting some of the rarer modes involving strange particles. Charges of produced pions are slightly skewed towards  $\pi^-$  in view of the ‘brought in’ negative charge. Pion momenta are chosen from an inclusive distribution loosely based on experiment. The energy weighted distribution is normalized to twice the nucleon mass which predicts a multiplicity of 4.3—close to observation. In a complex nucleus the annihilation is treated as though it occurs on free nucleon except that each pion produced by the annihilation process

\* Work supported by the Universities Research Association, Inc., under contract DE-AC02-76CH00300 with the U. S. Department of Energy.

<sup>†</sup> Email: mokhov@fnal.gov

is given a 50% probability to interact within the nucleus. This shortcut attempts to include—at least qualitatively—participation by the constituent nucleons.

Total cross sections for  $\bar{p}A$  in flight are estimated from geometrical considerations and from  $\sigma_{\bar{p}p}$ ,  $\sigma_{\bar{p}n}$ ,  $\sigma_{pp}$ , and  $\sigma_{pn}$  data. Annihilation in flight uses the same (Lorentz transformed) inclusive pion distribution as annihilation at rest. Above 0.1 GeV/c a small  $\bar{p}p \rightarrow \bar{\pi}n$  component is included. Nuclear target effects are again approximated by allowing some re-interaction of emerging particles in the same nucleus. Quasi-elastic events of  $\bar{p}$ ,  $\bar{n}$  with target nucleons rely on MARS algorithms for  $pA$  and  $nA$  but with the fastest emerging nucleon identified as its antiparticle.

### 3 DOSE DISTRIBUTIONS

A few selected results on dose delivered to the TEP are presented. For lack of space these are restricted to absorbed dose [5]. To facilitate inter-comparison, the beam energy for each type of particle is chosen to have a range of 15 cm in tissue: 147.2 MeV for protons, 68.3 MeV for pions and 61.8 MeV for muons. Each beam is uniformly distributed over  $-0.5 \leq x, y \leq 0.5$  cm and is incident normally on a 30 cm slab TEP. A 70 MeV neutron beam is included for a comparison. Fig. 1 shows the absorbed energy as a function of depth for each beam. Isodose contours for absorbed dose produced by the  $p$ ,  $\pi^-$ , and  $\mu^-$  beams are presented in Fig. 2. In Fig. 3 the laterally integrated dose due to  $\pi^-$  and  $\mu^-$  beams of the above energy is analyzed into its main contributing mechanisms. In both cases ionization losses are the main contribution up to and including the Bragg peak. For  $\pi^-$  there is comparable contribution near the peak from high-dE/dx charged particles associated with capture. Decay of the pions results in muons depositing 3.17 and 0.49 MeV for  $\pi^+$  and  $\pi^-$  while neutrinos carry away 60.2 and 0.49 MeV, respectively. For  $\mu^-$  the second largest dose contribution is due to electrons from  $\mu$  decay and the showers induced by them.

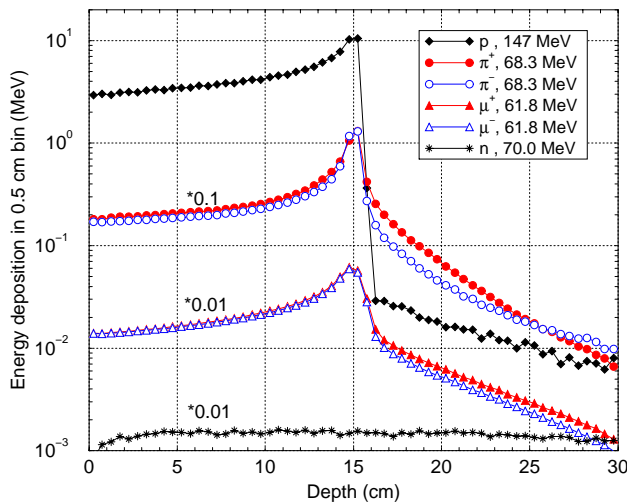


Figure 1: Laterally integrated absorbed energy in a TEP for proton, pion, muon and neutron  $1 \times 1$  cm beams.

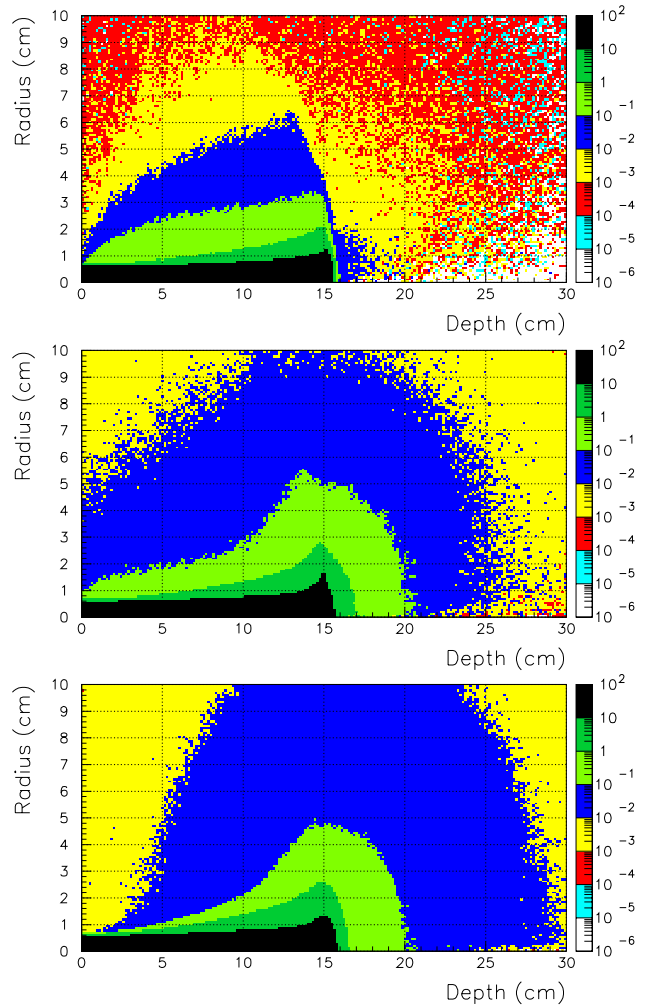


Figure 2: Absorbed isodose contours ( $nrad$  per incident particle) in a TEP for 147.2 MeV  $p$  (top), 68.3 MeV  $\pi^-$  (middle) and 61.8 MeV  $\mu^- 1 \times 1$  cm beams.

As a rough measure of effectiveness of the various particle beams one may compare dose delivered at entrance with that at the peak. The entrance dose can be regarded as a general proxy for dose delivered to healthy tissue and—in addition—is of particular interest in connection with the ‘skin sparing effect’ [2]. In this regard it makes sense to compare the ratio of *peak absorbed dose*, as a measure of radiotherapeutic effectiveness, to *entrance dose equivalent* as a measure of damage to healthy tissue (and in particular to the skin). This comparison is shown in Table 1 for doses averaged over  $\Delta r$  about the beam axis and over a depth of  $\Delta z$  near the peak for two cases: (1)  $\Delta r = \Delta z = 0.5$  cm and (2)  $\Delta r = \Delta z = 1.5$  cm. These can be thought to represent tumors with volume of 0.39 and 10.6  $\text{cm}^3$ , respectively. It is seen that by this measure  $\pi^-$  are most effective although, except for neutrons, the other beams come close—particularly for the larger region.

A stopping  $\mu^-$  attaches more readily to a heavy nucleus than to a light one—such as found in tissue. To exploit this one might inject a heavy element or compound, in a slurry or solution, into the tumor region prior to irradiation. Such

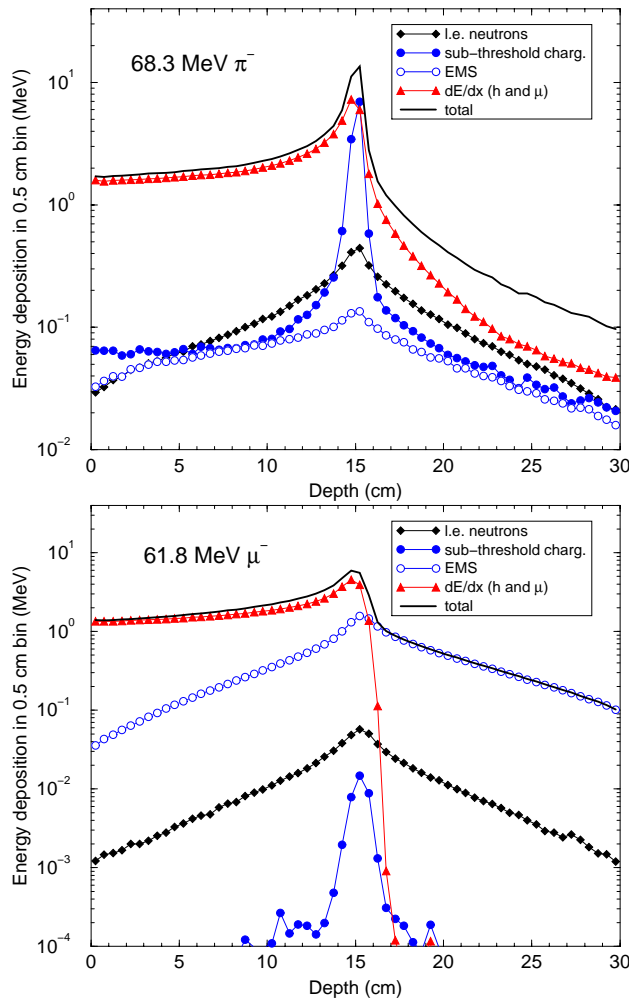


Figure 3: Laterally integrated absorbed energy and its components for 68.3 MeV  $\pi^-$  (top) and 61.8 MeV  $\mu^-$  (bottom).

an agent must be chosen with some care not only with regard to its effectiveness in delivering a larger dose but also to its toxicity, residual radioactivity produced, capability for removal after irradiation, etc. To obtain a preliminary indication we tried a  $BaI_2$  solution of a density  $1.67 \text{ g/cm}^3$ , present in a 1.5 cm region around the dose peak. Fig. 4 shows that peak dose increases by about 30%. This strategy would have much less effect for  $\pi^-$  where capture is assured even for light nuclei.

Table 1: Peak absorbed dose to entrance dose equivalent

Case	$p$	$\pi^+$	$\pi^-$	$\mu^+$	$\mu^-$	$n$
1	1.31	1.00	1.42	0.73	0.71	0.08
2	2.03	2.55	2.97	2.52	2.49	0.12

## 4 CONCLUSIONS

The various beams available in connection with a muon collider might be of considerable interest to radiotherapy. En-

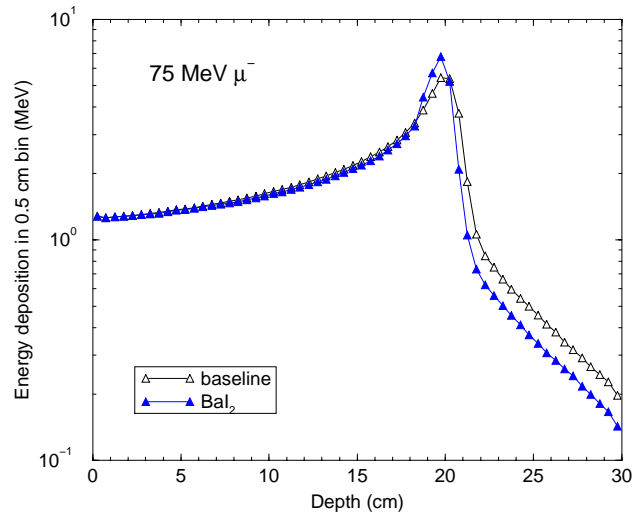


Figure 4: Laterally integrated absorbed dose for a 75 MeV  $\mu^-$   $1 \times 1$  cm beam in a standard TEP and in one with  $BaI_2$  solution at  $18.5 \leq z \leq 20.5$  cm and  $r \leq 1.5$  cm.

ergy deposition distribution in a TEP induced by various beams show substantially different patterns which might be exploited by the therapist. Negative pion beams provide the best peak-to-entrance dose ratio but pure  $\pi^-$  beams are difficult to prepare. Cooled muon beams could rival proton beams with regard to purity and deliver a better peak-to-entrance ratio—particularly for larger tumors. Muon dose appears also to be more uniformly distributed compared with protons. An important aspect would be the ability to evaluate and intercompare the efficacy of the various beams in a common setting which might be provided by a muon collider complex.

## 5 REFERENCES

- [1] C. M. Ankenbrandt et al., "Status of Muon Collider Research and Development and Future Plans", Fermilab-Pub-98/179 (1998).
- [2] P. L. Petti and A. J. Lennox, "Hadronic Radiotherapy", *Annu. Rev. Nucl. Part. Sci.*, **44**, 155-197 (1994). We wish to thank A. J. Lennox for useful discussion.
- [3] N. V. Mokhov, S. I. Striganov, A. Van Ginneken, S. G. Mashnik, A. J. Sierk, and J. Ranft, "MARS Code Developments", Fermilab-Conf-98/379 (1998); LANL Report LA-UR-98-5716 (1998); *nucl-th/9812038 v2 16 Dec 1998*; <http://www-ap.fnl.gov/MARS/>.
- [4] S. G. Mashnik, "User Manual for the Code CEM95", JINR, Dubna, 1995; OECD Nuclear Energy Agency Data Bank, Paris, France, 1995; <http://www.nea.fr/abs/html/iaea1247.html>; RSIC-PSR-357, Oak Ridge, 1995.
- [5] Radiotherapists make use of an RBE-factor (relative biological effectiveness) in their evaluation of various beams but these factors are not readily applied to our calculations since they depend not only on particle type and energy but also on the time structure (fractionation) and absolute level of dose delivered. Overall, RBE-enhanced dose appears to resemble absorbed dose better than dose equivalent.